Modeling of finishing force and torque in ultrasonic-assisted magnetic abrasive finishing process

Aviral Misra[1], Pulak Mohan Pandey[1], Uday S Dixit[2], Anish Roy[3] and Vadim V Silberschmidt[3]

A new finishing technique called ultrasonic-assisted magnetic abrasive finishing integrates ultrasonic vibration with magnetic abrasive finishing process for finishing of workpiece surface more efficiently as compared to magnetic abrasive finishing in the nanometer range. During finishing, two types of forces are generated in ultrasonic-assisted magnetic abrasive finishing, namely, a normal force (indentation force) and a tangential force (cutting force) that produces a torque. The finishing forces have direct control on the rate of change of surface roughness and material removal rate of the workpiece surface. This article deals with the theoretical modeling of the normal force and the finishing torque based on the process physics. In this work, finite element simulations of the electromagnet were performed to calculate a magnetic flux density in the working zone; they were also used to evaluate the normal force on the workpiece surface. The theory of friction for the abrasion of metals was applied together with the effect of ultrasonic vibration to calculate the finishing torque. The developed model predicts the normal force and finishing torque in ultrasonic-assisted magnetic abrasive finishing as functions of the supply voltage, working gap and concentration of abrasive particles in a flexible magnetic abrasive brush. A comparison of theoretical and experimental results is performed to validate the proposed model.

Keywords
Ultrasonic-assisted magnetic abrasive finishing, magnetic abrasive finishing, finishing, modeling, forces, torque, simulation

Introduction

With present technological advancements, there is a great need for a wide range of industries to have fine finishing capabilities which can produce surface roughness in nanometer range. There were many developments over the last few decades in the cost-effective and quality-assured manufacturing of precisely finished components for a variety of industrial applications.[1,2] There are a number of finishing processes involving the use of abrasives, for example, abrasive flow machining,[3–5] magneto-rheological fluid-based machining[6,7] and magnetic abrasive finishing (MAF).[8] In MAF, the finishing forces are primarily controlled by the magnetic field produced by a permanent magnet or an electromagnet.[9] The MAF process gained popularity in the industrial application as it can be used for finishing of both ferromagnetic and non-ferromagnetic materials. In this process, a flexible magnetic abrasive brush (FMAB) is formed that finishes the surface. The process has several advantages over bonded abrasive processes such as grinding. Some of these are self-adaptability of finishing tool, self-sharpening of abrasives and no requirement of dressing.[1,10,11] However, it was found that MAF was less efficient with regard to the rate of improvement in the surface finish when used for finishing of materials with high hardness values.[12,13] Many variants of MAF were developed to reduce this shortcoming and also to enhance the process

[1]Department of Mechanical Engineering, Indian Institute of Technology Delhi, New Delhi, India
[2]Department of Mechanical Engineering, Indian Institute of Technology Guwahati, Guwahati, India
[3]The Wolfson School of Mechanical, Electrical and Manufacturing Engineering, Loughborough University, Loughborough, UK

Corresponding author:
Pulak Mohan Pandey, Department of Mechanical Engineering, Indian Institute of Technology Delhi, New Delhi 110016, India.
Email: pmpandey@mech.iitd.ac.in

capabilities; ultrasonic-assisted magnetic abrasive finishing (UAMAF) process is one such development in this direction.[14]

UAMAF is a hybrid finishing process in which ultrasonic vibration is introduced into a finishing zone of the MAF process to obtain improved surface topology within a reasonably short period of time. It was found experimentally that the UAMAF process provided better performance than a conventional MAF process. UAMAF could produce a finished surface with roughness value of 22 nm using unbonded or loose magnetic abrasive particles (UMAPs) with AISI 52100 as the workpiece material.[15] A schematic of the UAMAF setup is shown in Figure 1. The electromagnet had four poles alternately arranged as north and south poles, and ultrasonic vibration was applied to the workpiece fixture by a horn attached to a transducer. The workpiece fixture was mounted on a dynamometer assembly to monitor the magnitude of finishing forces and torque during experimentation. In UAMAF, nano-scratching and micro-chipping by abrasive particles, additionally enhanced due to ultrasonic vibrations, were responsible for material removal from the workpiece surface.[16] Forces encountered during the finishing had a direct influence on quality and exactitude of the finished surface. Hence, it is imperative to have an in-depth understanding of the forces involved in UAMAF. Finishing forces in UAMAF were induced as a result of the interaction of FMAB with the workpiece surface in the presence of ultrasonic vibration. The strength of the FMAB depended upon the magnetic field produced by the electromagnet, a higher strength of FMAB resulting in a higher finishing force during the process. There were two main finishing forces during UAMAF process, namely, a normal force and a tangential force. The normal force (F_n) was caused by the strength of the magnetic field in the working zone and was responsible for indentations of abrasive particles on to the surface of workpiece. The tangential force (F_t) was responsible for shearing off irregularities from the workpiece surface; it was a resultant of forces generated by rotation of the FMAB and ultrasonic vibration.

The first successful attempt to model an MAF process was made by Shinmura et al.[17] They developed equations for finishing forces on a cylindrical workpiece and estimated the magnetic pressure created by abrasive particles on the workpiece surface. Their model provided the good qualitative agreement with the experiments. Another model for the evaluation of magnetic finishing pressure on the workpiece surface was developed by Khairy.[18] He modeled kinematics of the MAF process analytically by considering similarities of the cutting zone of belt or form grinding with that of MAF and validated the model with experiments on steel bars. Mori et al.[19] explained the formation of the FMAB from the standpoint of brush formation energy considering varying weights of magnetic abrasive particles. The mechanism of MAF was described on the basis of normal and tangential forces acting on the edges of FMAB. The calculated values of normal force agreed well with the measured ones.

A theoretical model to estimate the finishing pressure, surface roughness and finishing time for a tool–workpiece interaction in a cylindrical MAF process was estimated by Kim and Choi.[20] They deduced that the strength of magnetic flux density in the working gap was greatly affected by the magnitude of the gap. A finite element analysis (FEA) of magnetic field for the prediction of magnetic potential in the working gap was carried out by Jayswal et al.[21] to calculate normal and tangential forces in the case of the MAF process. They also discussed different conditions of the finishing forces for the removal of material from the workpiece. Kala et al.[22] modeled normal and tangential forces in double-disk MAF process considering the analogy of a string fixed at two ends under tension. The equations of Lorentz force and the Ampere's law were used to calculate the forces. They used experimental data to incorporate the effect of magnetic flux density and angle of inclination of FMAB chains. The model was validated using experimental results.

The literature survey indicates that attempts[17–22] were made to predict the finishing forces during MAF. First attempt to model UAMAF process was made by Mulik and Pandey.[23] They developed a model for the prediction of finishing force and torque as functions of the supplied voltage, working gap and hardness of the workpiece surface. They assumed abrasive grains of a tetrahedral shape and tangential force exerted by the indented part of grains as a shear force on the workpiece material. The effect of ultrasonic vibration on the finishing torque was calculated based on its impulse. The developed model of normal force and finishing torque was in good agreement with the experimental results.

In this work, an improved model of UAMAF for the estimation of finishing force and torque was developed. The novelty of this model compared to existing model is as follows:

- The average magnetic flux density on the surface of the workpiece is obtained by finite element simulation.
- A body-centered cubic (BCC) structure is assumed for the arrangement of ferromagnetic and abrasive particles throughout the working gap.
- The effect of ultrasonic vibration on the finishing torque is assessed by considering the relative velocity of abrasive particles and the workpiece surface, unlike considering only the impulse of vibration to incorporate its effect.
- The theory of abrasion in metal is used for the calculation of friction between the FMAB and the workpiece surface.

The developed model was used to predict the normal force and finishing torque considering the voltage,

working gap and concentration of abrasives as significant parameters. It was validated with the experiments.

Modeling of finishing force and torque

The mechanism for the formation of the FMAB and its interaction with the workpiece surface is a complex system; hence, to simplify the mathematical modeling of the finishing force and torque, the following realistic assumptions are made:

1. All the ferromagnetic and abrasive particles are considered spherical in shape. Although these particles are of varied shape due to the differences in their corresponding manufacturing methods, this assumption saves the modeling effort substantially and relinquishes the problem of obtaining a large amount of data regarding the shape of the particles, since particles can be characterized by a unique parameter, that is, the grain diameter.[24] Also, the orientation of active abrasive grains on the surface of the workpiece is rendered inconsequential.
2. The size of ferromagnetic and abrasive particles depends on their mesh or sieve number and remains uniform throughout the FMAB. The diameter of abrasive (D_a) or ferromagnetic (D_f) particles can be related to the mesh number (M) as D_f or $D_a = 0.6/M \times 25.4$ (mm), and if abrasive particles are specified in terms of a range of the mesh number, then the size distribution is assumed to be normal and is symmetric about the mean particle diameter (D_a) given by $D_a = 7.62(M_a + M_b/M_aM_b)$(mm), where M_a is the lower mesh number, allowing all the grains to pass through the sieve, and M_b is the upper mesh number, detaining most of the grains in the sieve.[24]
3. The ferromagnetic chains formed are continuous and remain unaffected by the presence of nonmagnetic abrasive particles and rotation of the electromagnet.
4. A magnetic flux density is uniformly distributed over the workpiece surface and also does not vary with time. Its magnitude, for theoretical calculations, is the average of values obtained from simulations at different locations on the surface of the workpiece under the FMAB.
5. The properties of UMAPs do not change during the process. As UAMAF has a low material removal rate, the removed material mixed with UMAPs does not significantly alter properties of the FMAB.
6. Only a fraction of the abrasive particles that are in contact with the workpiece surface takes part in cutting action, and those particles are known as active abrasive particles.
7. The FMAB consists of abrasive and ferromagnetic particles without voids.

Finite element simulation of magnetic field

Distribution of the magnetic field in the finishing zone significantly affects the finishing characteristics of the process.[20] Its distribution in the machining gap determines the configuration and rigidity of the FMAB for the finishing operation.[25] The magnetic field distribution in the working gap includes the magnitude of magnetic flux density as well as its gradient. It depends on the shape, size, the material of the magnetic poles, supplied voltage (or current) to the coils of the electromagnet and the relative position of magnetic poles with regard to the workpiece. Indentation of an active abrasive particle into the workpiece surface is due to the normal force applied to it by surrounding magnetized ferromagnetic particles as a result of the magnetic levitation force.[6] All the above factors are important to calculate the magnetic force acting on active abrasive particles, producing finishing pressure on the surface of the workpiece during UAMAF. When a voltage (or current) is applied to the electromagnet, a magnetic field is created in the working gap. Higher the magnetic flux density, the higher is the strength of the FMAB and the higher are the forces acting during the interaction of FMAB and surface of the workpiece. To determine the magnetic flux density ($\boldsymbol{B}$) in the finishing zone, FEA of the electromagnet was performed. A finite element simulator for electromagnetic problems, Ansoft Maxwell V13, was used for this purpose. The simulation results provided the magnetic flux density at different locations on the surface of the workpiece. The magnetostatic solver used the following Maxwell equations of magnetism for steady-state condition $\nabla \times \boldsymbol{H} = \boldsymbol{J}$ and $\nabla \times \boldsymbol{B} = 0$. The constitutive (material) relationship is $\boldsymbol{B} = \mu_0(\boldsymbol{H} + \boldsymbol{M})$, where $\boldsymbol{H}$ is the magnetic field intensity, $\boldsymbol{J}$ is the DC current density field flowing in the direction of transmission, $\boldsymbol{B}$ is the magnetic flux density and $\boldsymbol{M}$ is the magnetization vector or the magnetic dipole moment per unit volume. The magnetic flux density $\boldsymbol{B}$ was considered continuous across the boundary at the interface between the different components. Also, the magnetic field $\boldsymbol{H}$ was tangential to the region other that the electromagnet assembly; magnetic flux could not cross the region. Mathematically, $\boldsymbol{a_n} \times (\boldsymbol{H}_1 - \boldsymbol{H}_2) = \boldsymbol{J}$ and $\boldsymbol{a_n}.(\boldsymbol{B}_1 - \boldsymbol{B}_2) = 0$, where $\boldsymbol{a_n}$ is the unit normal vector to the surface and directed form body 1 to body 2, indices 1 and 2 denote fields in body 1 and 2.

A computer-aided design (CAD) model of electromagnet was developed (refer Figure 1) in the software. The length and cross section of the magnet were 55 mm and 25 mm × 15 mm, respectively, with the diameter of the magnet core as 80 mm. The relative permeability of the core (iron) was 4000, conductivity of coils (copper)

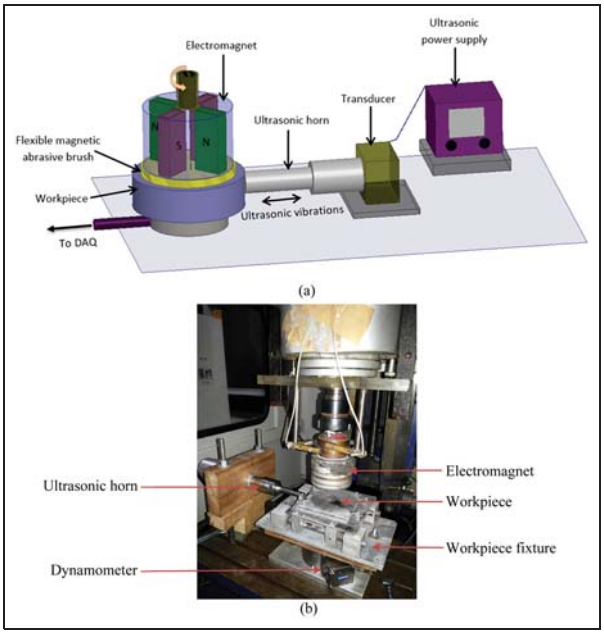

Figure 1. Experimental setup used to estimate normal force and finishing torque during UAMAF: (a) schematic diagram and (b) actual system.

58×10^6 S/m and the relative magnetic permeability of working gap (air) was 1. Different excitations in the range of 20–100 V were applied to the coils of the electromagnet to get the magnetic flux density on the surface of the workpiece considering different working gaps in the range of 1–2.5 mm. The element used in numerical simulations was a tetrahedron with the field approximated over it as a second-order basis function to account for geometrical complexities and also to improve the accuracy of the solution. The final solution was obtained using an iterative solution method, with an initial mesh generated based on a surface approximation and further refinement of mesh occurring in regions with an error in energy norm higher than 1%. The value of error in the energy norm was computed after each solution step and used as a measure of convergence for the refined mesh. The total of 20 iterative steps was performed to get the final solution. In total, 192,189 tetrahedral elements were created in the final step.

A contour plot of magnetic flux density on the surface of the workpiece and magnetic lines of forces created in the working gap as observed in the final step of simulations are depicted in Figure 2(a). From Figure 2(a), it can be seen that the magnetic flux density was higher under the poles than elsewhere and has similar variation under every pole. A surface plot under the magnetic pole (Figure 2(b)) is drawn from the simulation data in order to conceptualize correct variation of magnetic flux density. The magnetic flux distribution was observed to have different magnitudes varying with the location under the pole. Hence, for calculation of the average magnetic flux density, the magnitude of magnetic flux density was considered at the interval of

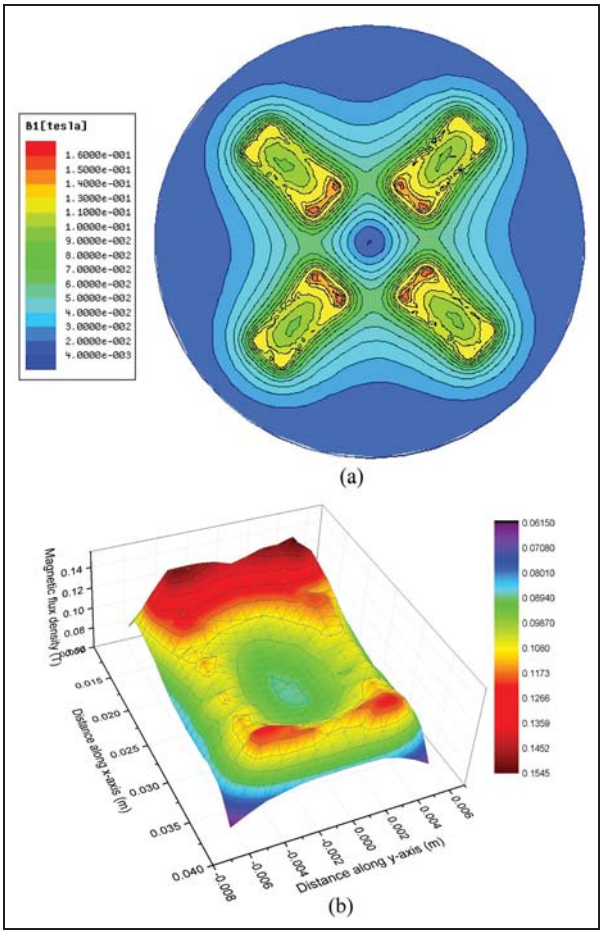

Figure 2. (a) Contour plot of magnetic flux distribution on surface of workpiece and (b) surface plot of magnetic flux density under one pole.

1 mm throughout the rectangular area of the slot, and its average value was calculated.

Number of active abrasive particles

The normal force acting on abrasive particles will force them to indent on to the workpiece surface, and the relative motion (due to tangential force) between these abrasive particles and workpiece surface will shear off the material in front of the indented portion of the abrasive particle as micro/nano-scratching. Only a few abrasive particles come in contact with the workpiece surface and actually take part in the finishing action; these are known as "active abrasive particles". Hence, for the development of any theoretical model for calculation of forces, material removal or surface roughness in UAMAF, the assessment of active abrasive particles is a necessary step. UMAPs are a blend of ferromagnetic and abrasive particles. In UMAPs, abrasive and ferromagnetic particles are randomly arranged. When the magnetic field is activated, the ferromagnetic particles in UMAPs orient themselves in the form of chains along the magnetic lines of force. The chains are formed as a result of interaction between the magnetic dipoles

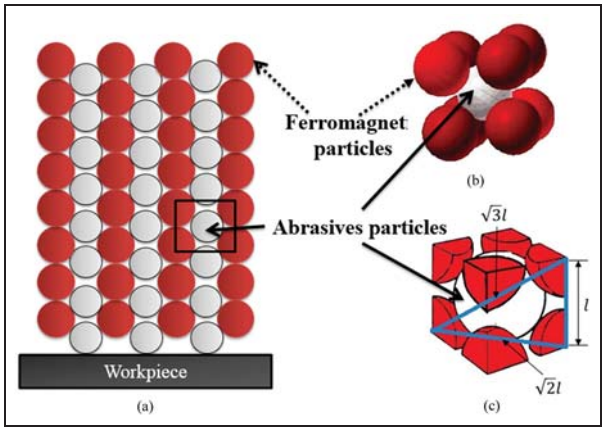

Figure 3. (a) Schematic of two-dimensional arrangement of chains comprising ferromagnetic and abrasive particles on enactment of magnetic field, (b) an arrangement of abrasive and ferromagnetic particles in 3D BCC structure and (c) BCC unit cell considered for modeling.

of ferromagnetic particles due to the application of magnetic field.[26] The stable brush forms only when the magnetic energy required for its formation is the minimum;[19] the minimum value of dipolar energy occurs when dipoles join each other and align along the direction of field forming the chains of ferromagnetic particles.[27] The abrasive particles of non-magnetic nature get entrapped between these chains of ferromagnetic particles thus forming the FMAB (Figure 3(a)). The magnetic energy present in the FMAB is used to grip non-magnetic abrasive particles; at the equilibrium condition, the FMAB also attains the minimum energy.[19] Due to the presence of non-magnetic abrasive particles, chains are hardly continuous and form a complex structure combining ferromagnetic and abrasive particles. Considering, these facts and to simplify the analysis, it was assumed that an abrasive particle in combination with eight ferromagnetic particles forms a BCC structure with ferromagnetic particles at eight corners of the cube and the abrasive particle remaining at its center[28] as shown in Figure 3(b). Hence, a uniformity throughout the FMAB can be observed. Assuming BCC structure implies that abrasive particle is rigidly entrapped between the ferromagnetic particles and no relative motion between them is possible since ferromagnetic particles attain the position along the magnetic lines of forces. It also implies that the force from any direction (horizontal or vertical) that acts on ferromagnetic particles is completely transmitted to the adjacent abrasive particle. Due to large number of random abrasive and ferromagnetic particles, the above assumptions may be reasonable. It was also assumed that this unit of BCC cells was uniformly distributed throughout the workpiece surface.

As shown in Figure 3(c), one BCC unit has one abrasive grain in it. The total number of BCC units on the surface of the workpiece is the ratio of area of the brush in contact with the surface of workpiece to the area of the face of one BCC unit, which depends on the size of ferromagnetic and abrasive particles. The length of the unit BCC cell (l) can be calculated as follows

$$l = \frac{D_a + D_f}{\sqrt{3}} \tag{1}$$

D_a and D_f are the diameters of the abrasive and ferromagnetic particles, respectively.

The area of the brush A_{brush} in contact with the surface of the workpiece is given by assuming that the effective magnetic field for creating sufficient forces for finishing occurs only under the pole of the magnet

$$A_{brush} = \text{area of single pole} \times \text{number of poles} \times \eta_b \tag{2}$$

where η_b is the factor that takes into account the deviation of the actual area of the brush involved in finishing as compared to the area of the pole of the electromagnet, which is the source of magnetic energy for the formation of the FMAB. The factor η_b is the ratio of actual area of the brush in contact with the workpiece surface A_w to that of the pole of electromagnet A_p and can be written as

$$\eta_b = \frac{A_w}{A_p} \tag{3}$$

Here, for simplicity, η_b is assumed to be equal to 1 as there was a high magnetic field under the poles of electromagnet only that vanishes away from the pole (Figure 2(a)). Hence, the number of active abrasive particles n_a is given as

$$n_a = \frac{A_{brush}}{l^2} \tag{4}$$

Volume fraction of ferromagnetic particles

The volume fraction of ferromagnetic particles can be calculated from the weight fraction of abrasive particles (or concentration) C as follows. The density of the brush (ρ_{brush}) is given by

$$\rho_{brush} = \frac{100 \times \rho_{abrasive} \times \rho_{ferro}}{C \times \rho_{ferro} + (100 - C) \times \rho_{abrasive}} \tag{5}$$

where C can be calculated as $C = (m_a/m_a + m_f) \times 100$, where m_a is the weight of abrasive particles, m_f is the weight of ferromagnetic particles; $\rho_{abrasive}$ is the density of the abrasive particles; and ρ_{ferro} is the density of ferromagnetic particles. The volume of ferromagnetic particles in FMAB is

$$V_{ferro} = \frac{(100 - C) \times \rho_{brush} \times V_{brush}}{100 \times \rho_{ferro}} \tag{6}$$

where V_{brush} is the volume of the brush and is given as

$$V_{brush} = A_{brush} \times \text{working gap} \tag{7}$$

Hence, from equations (5)–(7), the volume fraction of ferromagnetic particles (α) is given by

$$\alpha = \frac{V_{ferro}}{V_{brush}} \tag{8}$$

Calculation of average normal force

The magnetic flux density calculated in section "Finite element simulation of magnetic field" on the surface of the workpiece was used to estimate pressure on this surface. The average normal pressure (P_m) exerted by the FMAB on the surface of the workpiece can be expressed by the following equation[17]

$$P_m = \frac{B^2}{4\mu_0} \times \frac{3\pi(\mu_{FP} - 1)\alpha}{3(2 + \mu_{FP}) + \pi(\mu_{FP} - 1)\alpha} \tag{9}$$

where B is the average magnetic flux density on the surface of the workpiece, μ_0 is magnetic permeability in vacuum ($4\pi \times 10^{-7}$ N/A^2), μ_{FP} denotes magnetic permeability of ferromagnetic particles and α is the volume fraction of ferromagnetic particles in the FMAB. Therefore, the average normal force exerted by the FMAB is given by[23]

$$F_N = P_m \times A_{brush} \tag{10}$$

Thus, the average normal force by a single abrasive particle (f_N) on the surface of the workpiece can be calculated as

$$f_N = \frac{F_N}{n_a} \tag{11}$$

Calculation of average finishing torque

The normal force calculated in section "Calculation of average normal force" developed due to the magnetic field acting on abrasive particles results in their indentation into the workpiece surface. The relative motion between the indented abrasive particles and workpiece surface causes a resisting force tangential to the surface. To overcome this resisting force, a torque has to be provided to the electromagnet, which is called finishing torque. The cross-sectional view of an indented active abrasive particle into the workpiece surface is shown in Figure 4. The extent of indentation of abrasive particles depends upon the magnitude of the normal force and hardness of the workpiece material.[27] When the tangential force is applied to abrasive particles, due to rotation of the electromagnet, the workpiece material in front of the indented portion resists the motion of abrasive. This resistance depends directly on the magnitude of the normal force (or indentation force). When the tangential force is sufficient to overcome this resistance, the abrasive plows the material in front of it causing abrasion of the workpiece on its surface. Bowden et al.[29] stated that the frictional force was not only a surface effect but also depended upon the bulk properties of sliding bodies. They described that the frictional resistance between the sliding bodies was essentially caused by the shearing of metallic junctions formed due to adhesion or welding at contact points and also due to the resistance force of plowing of the surface irregularities of the softer metal by the harder one.

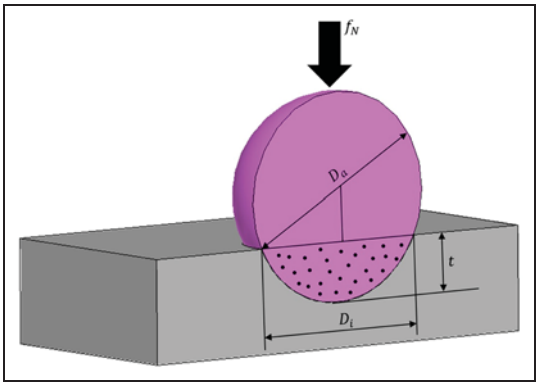

Figure 4. Schematic of cross-sectional view of an active abrasive particle indented into surface of workpiece.

When an indented active abrasive particle is provided a relative motion tangential to the workpiece surface, plowing and adhesion phenomena cause friction between the abrasive and the workpiece. The coefficient of friction depends on the shape and size of the abrasive particle.[30] Here, it is assumed that the frictional force acting between the FMAB and the workpiece surface is caused by plowing and adhesion. The friction force during the interaction of the FMAB and the workpiece surface is derived below. The force on single abrasive particle is given by[31]

$$f_N = \sigma_w \Delta A \tag{12}$$

where

$$\Delta A = \frac{\pi D_i^2}{4} \tag{13}$$

where ΔA is the area of indentation and σ_w is flow stress of the workpiece material, which is related to its Brinell hardness (H_w) by the following equation[32]

$$\sigma_w = KH_w \tag{14}$$

Here, $K = 1$ for brittle material and $K > 1$ for ductile material (for steel $K = 3.0$). Hence, from equations (12)–(14), the diameter of indentation by the abrasive particle into the workpiece surface can be calculated as

$$D_i = 2\sqrt{\frac{f_N}{\pi K H_w}} \tag{15}$$

The coefficient of friction due to plowing and adhesion of a sphere on a flat surface is

$$\mu = \mu_p + \mu_a \tag{16}$$

Here, μ_p is the plowing friction coefficient and μ_a is the adhesion friction coefficient, where the former is given by[30]

$$\mu_p = \left(\frac{2}{\pi}\right)\left[\left(\frac{D_a^2}{D_i^2}\right)\sin^{-1}\left(\frac{D_i}{D_a}\right) - \sqrt{\left(\frac{D_a^2}{D_i^2}\right) - 1}\right] \quad (17)$$

and the latter is[30]

$$\mu_a = \mu_{mm}\left(\frac{4D_a^2}{\pi D_i^2}\right)\left[1 - \sqrt{1 - \left(\frac{D_i}{D_a}\right)^2}\right] \quad (18)$$

Here, D_a is the diameter of the abrasive particle, D_i is the diameter of the indentation (see Figure 4) and μ_{mm} is the coefficient of friction of the workpiece material whose value is taken as 0.3.[33] Then, the total friction force (F_0) caused by all active abrasives responsible for a torque between the FMAB and the workpiece is

$$F_0 = n_a f_0 = \mu f_N n_a \quad (19)$$

The torque T_{MAF} without ultrasonic vibration produced by the electromagnet is given by

$$T_{MAF} = F_0 r_{mean} \quad (20)$$

Here, r_{mean} is the mean radius of the electromagnet which can be calculated by assuming a uniform wear theory,[34] that is

$$r_{mean} = \frac{r_{outer} + r_{inner}}{2} \quad (21)$$

where r_{outer} and r_{inner} are the outermost and innermost distance of the pole from the center of the electromagnet, respectively. The torque in equation (20) was calculated for a case when no ultrasonic vibration was applied in the finishing zone; hence, this torque is for plane MAF. To calculate torque during UAMAF, the effect of ultrasonic vibrations should be considered; it is discussed in the following section.

Effect of ultrasonic vibrations on finishing torque

In UAMAF, the FMAB rotates with a constant angular speed about Z-axis, and a vibratory motion with amplitude A and frequency f is provided by the ultrasonic horn along X-axis. Kumar and Hutchings[35] proposed a theory, which states that vibration affects the friction force exerted on the body whether its sliding velocity is collinear or normal to the vibration direction. Hence, the effect of ultrasonic vibration on the frictional force was calculated by imposing ultrasonic vibration on the sliding abrasive. Active abrasive particles in the FMAB slide with different tangential velocities and follow different tracks. For simplicity, it is assumed that all the active abrasive particles have constant tangential velocity V_r on the surface of the workpiece due to rotation of magnet, and its magnitude is given by $V_r = (2\pi N r_{mean}/60)$ (m/s), where N is the number of revolutions per minute of the electromagnet. Over one rotation of the magnet, the velocity V_r changes its direction with respect to the direction of vibration. Hence, the effect of ultrasonic vibration was formulated by dividing the problem into two cases by considering two components of V_r. One component V_x is along X-axis (i.e. along the direction of vibration) and other is V_y along Y-axis (i.e. perpendicular to the direction of vibration), where $V_x = V_r\cos\theta$ and $V_y = V_r\sin\theta$ (θ is instantaneous angle between V_r and direction of vibration as shown in Figure 5). Now in Case 1, the component of velocity of abrasive particle along the direction of vibration is considered, and in Case 2, the component of velocity of abrasive particle perpendicular to the direction of vibration velocity is taken. Then, effect of ultrasonic vibrations is calculated on the frictional force between FMAB and the workpiece surface in each case.

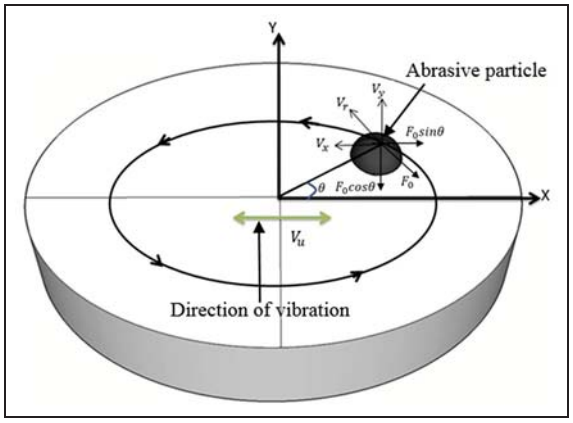

Figure 5. Schematic of track of indented active abrasive particle and components of rotational velocity and friction force.

The magnitude of total friction force F_0 remains constant but magnitude of components along X-axis and Y-axis directions will change with time. The magnitudes of components of the F_0 depends on the instantaneous value of θ and are given by $F_X = F_0\sin\theta$ and $F_Y = F_0\cos\theta$ (Figure 5). Here, for the simplification, it is assumed that the components of friction force remain constant over the whole range of θ and are given by the root mean square (RMS) value of their magnitude waveform created over the one rotation, that is, $F_X = F_Y = F_0' = (F_0/\sqrt{2})$.

Case 1: component of velocity along direction of ultrasonic vibration. The instantaneous velocity of ultrasonic vibration, that is, of the workpiece surface, is assumed to be given by the equation

$$V_u(t) = 2\pi f A\sin(2\pi f t) \quad (22)$$

where A and f are the amplitude and frequency of vibration, respectively (see Figure 6(a)). From equation (22), it is observed that the velocity vanishes at the ends and is the maximum in the middle of each cycle;

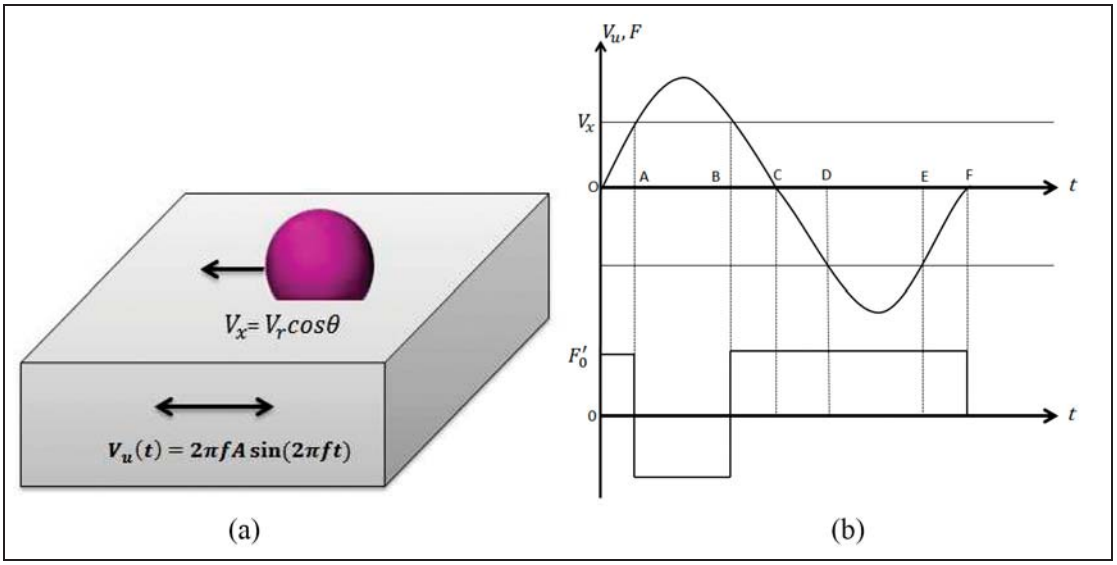

Figure 6. (a) Sliding of abrasive over workpiece surface with vibratory motion collinear with sliding velocity direction and (b) variation of instantaneous vibrational velocity of workpiece with time and corresponding change in friction force direction between abrasive and workpiece.

Figure 6(b) shows the variation of instantaneous velocity of workpiece and the change in friction force with time during one vibration cycle. Apparently, initially, the velocity keeps on increasing; at point A, it becomes equal to the component of sliding velocity (V_x). During the time interval OA, the friction force acts opposite to the direction of the component of sliding velocity (V_x) of the abrasive particle. After point A, the instantaneous velocity of workpiece, $V_u(t)$ is greater than V_x, and during interval AB it exceeds V_x; hence, there occurs a reversal of direction of the friction force, and it acts in the direction of V_x. The coefficient of friction is assumed to be independent of change in the relative velocity between the parts. During interval OA, $V_x > V_u(t)$, hence, the friction force acts opposite to the direction of V_x and is taken as positive. For interval AB, $V_x < V_u(t)$, the friction force acts in the same direction as V_x and is taken as negative. Over the remaining vibration cycle, V_x remains greater than $V_u(t)$, that is, for interval BF, the frictional force is positive. The frictional force acting during time intervals AB and DE are equal but opposite in direction; hence, when calculating average frictional force, their effects eliminate each other. Thus, only four remaining intervals OA, BC, CD and EF contribute to the friction force acting on the abrasive particles. The average frictional force acting during one vibration cycle was computed by considering these four time intervals.

The workpiece velocity $V_u(t)$ becomes equal to the sliding velocity V_x of the abrasive at any time $t = t_s$; hence, from equation (22), time t_s can be calculated as

$$t_s = \frac{1}{2\pi f}\sin^{-1}\left(\frac{V_x}{2\pi Af}\right) \tag{23}$$

The resultant averaged friction force (F_{xa}) acting over the complete cycle of vibration is given by[35]

$$F_{xa} = \frac{F_0'}{T}(4t_s) = F_0'\left(\frac{2}{\pi}\sin^{-1}\frac{V_x}{2\pi Af}\right) \tag{24}$$

where F_0' is the friction force that acts without vibrations and T is the time period of vibration. In present case, it was observed that the reduction in friction took place only when the component of velocity of the abrasive particles V_x was less than the maximum velocity of the vibration; otherwise, there was no effect of vibration on the change in friction.

Case 2: component of velocity perpendicular to direction of ultrasonic vibration. In Figure 7(b), V_{rr} represents the resultant velocity of the rotational velocity component V_y and the vibrational velocity $V_u(t)$ (refer Figure 7(a)). When vibrational velocity reaches its maximum value, it makes angle ψ with V_y. The frictional force acts opposite to the direction of resultant velocity V_{rr}. Therefore, in one vibrational cycle, the frictional force changes its direction from $(+\psi)$ to $(-\psi)$ in direction opposite to the velocity of sliding V_y. The included angle between the endmost directions of the line of action of the friction force is 2ψ as shown in Figure 7(b).

If, at any instant, ξ is the angle between vectors V_{rr} and V_y, the component of frictional force can be divided into two components along X- and Y-directions:

1. In the direction of the velocity component V_y of abrasive, that is, $F_y(t) = F_0' \cos\xi$.
2. In the direction perpendicular to V_y (i.e. in the direction of V_u), that is, $F_x(t) = F_0' \sin\xi$.

From Figure 7(b), ξ is given by

$$\xi = \tan^{-1}\left(\frac{V_u(t)}{V_y}\right) \tag{25}$$

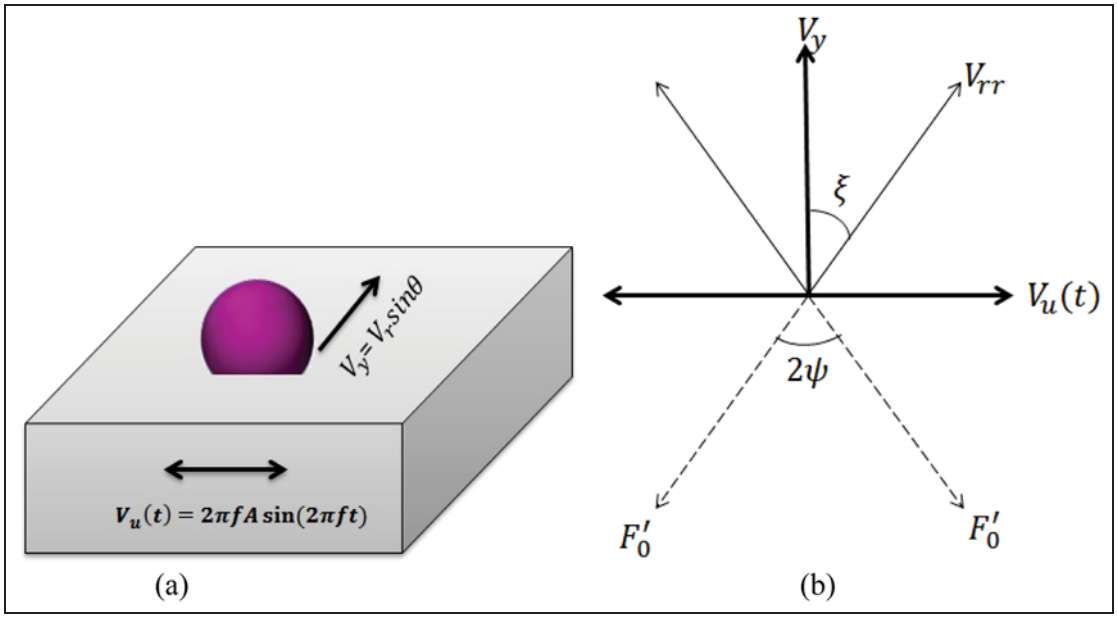

Figure 7. (a) Sliding of abrasive over workpiece surface with a vibratory motion perpendicular to sliding velocity direction and (b) relationship between vibrational velocity, sliding velocity, resultant velocity and direction of friction force, changing along angle 2ψ.

The instantaneous velocity of vibration vanishes at the phase angles 0, π and 2π; hence, vibration has no effect at these phase angles. The maximum velocity of vibration occurs at phase angle of $\pi/2$ and $3\pi/2$; for these phase angles, the variation resultant of the instantaneous frictional force due to ultrasonic vibration depends strongly on the ratio (V_u/V_y). From Figure 7(b), it can be easily concluded that the average value of the frictional force component $(F_x(t))$ along the direction of vibration vanishes for whole cycle of vibration. Hence, only the component of frictional force $F_y(t)$ has an effect over the complete cycle of vibration, and its average value can be calculated by integrating it over the time period for the cycle of vibration.

The average friction force over the complete time period for one cycle of vibration (F_{ya}) along the perpendicular to the direction of vibration is given by[35]

$$F_{ya} = \frac{1}{T}\int_0^T F_0' \cos\xi dt \tag{26}$$

From equations (25) and (22)

$$F_{ya} = \frac{1}{T}\int_0^T F_0' \cos\left(\tan^{-1}\left(\frac{2\pi Af\sin(2\pi ft)}{V_y}\right)\right)dt \tag{27}$$

Considering, the phase angle for the vibration cycle as $\varphi = 2\pi ft$, the above equation can be rewritten as

$$F_{ya} = \frac{1}{2\pi}\int_0^{2\pi} F_0' \cos\left(\tan^{-1}\left(\frac{2\pi Af\sin(\varphi)}{V_y}\right)\right)d\varphi \tag{28}$$

The above equation was computed numerically to get the averaged value of the friction force along the direction of V_y component of the sliding velocity. Form equation (27), it is concluded that as the ratio of vibrational velocity $V_u(t)$ to the velocity component V_y increases, there is a gradual decrease in the resultant average friction force F_{ya} over the time period of vibration cycle. As the ratio increases, there is considerable reduction in the computed frictional force.

The values of the average frictional force were computed in both the cases for a single cycle of vibration; a similar cycle is repeated over the whole finishing time. It is assumed that the force calculated for one cycle of vibration will remain constant. Hence, total average frictional force considering the effect of ultrasonic vibration is computed as

$$F_{au} = \sqrt{{F_{xa}}^2 + {F_{ya}}^2} \tag{29}$$

To calculate the above equation, forces F_{xa} and F_{ya} were computed using equations (24) and (28), respectively, to get the value of F_{au} at every angle between 0° and 90° at an interval of 1°. To simplify the calculation of the torque, the mean value F_{au} was taken. Hence, torque T_{UAMAF} due to the effect of ultrasonic vibration can be calculated as

$$T_{UAMAF} = F_{au} r_{mean} \tag{30}$$

This torque (T_{UAMAF}) had the lower magnitude as compared to the torque T_{MAF} calculated with equation (20) for the same set of process parameters. Hence, it was concluded that the torque produced in UAMAF had a smaller magnitude as compared to the torque produced during conventional MAF, which is validated by experiments.

Experimentation

The experimental setup used to measure finishing forces for the case of UAMAF is shown in Figure 1. The setup comprised a specially designed workpiece fixture, an ultrasonic vibration generator unit and dynamometer assembly. The assembly consists of a dynamometer (SCHUNK: Delta sensor with SI-330-30 Calibration), a data acquisition (DAQ) system and a data processor unit used to measure the normal force and finishing torque during UAMAF. The complete UAMAF setup was installed on a computer numerical control (CNC) milling machine. The electromagnet was mounted on the spindle to get the rotational motion. The working gap was maintained along Z-axis between the horizontal workpiece surface and the electromagnet. The ultrasonic vibratory motion was given to the workpiece in X-direction, and the electromagnet provided rotatory motion through the spindle with Z-axis as the axis of rotation. The experiments were carried out using three different parameters—supply voltage, working gap and mass fraction of abrasive in FMAB. The UMAPs prepared for experimentation contained different concentrations of abrasive particles (SiC) ranging from 15% to 30% of the total weight of UMAPs, which was 8 g, with the size of ferromagnetic particles of 300 mesh size and SiC particles of 400 mesh size. As already reported, the abrasive grain size has an insignificant effect on the finishing forces;[23] hence, the size of abrasive particles was kept constant. The workpiece material used for experiments was AISI 52100 steel with the hardness value of 61 HRC or 670 BHN. The DAQ was used to record the data for the normal force and the finishing torque about the Z-axis from the dynamometer; Figure 8(a) and (b) shows typical plots of the measured data for the normal force and the finishing torque, respectively, at 60 V, 1.5-mm gap and T_{on} = 2 s and T_{off} = 2 s.

From Figure 8(a), it can be observed that there is no significant variation in the normal force during T_{on} and T_{off} during finishing. Hence, the normal force was assumed to be constant during the finishing, and its magnitude was the average of all the values obtained during experimentation. When ultrasonic vibration was applied, the torque increased rapidly due to the

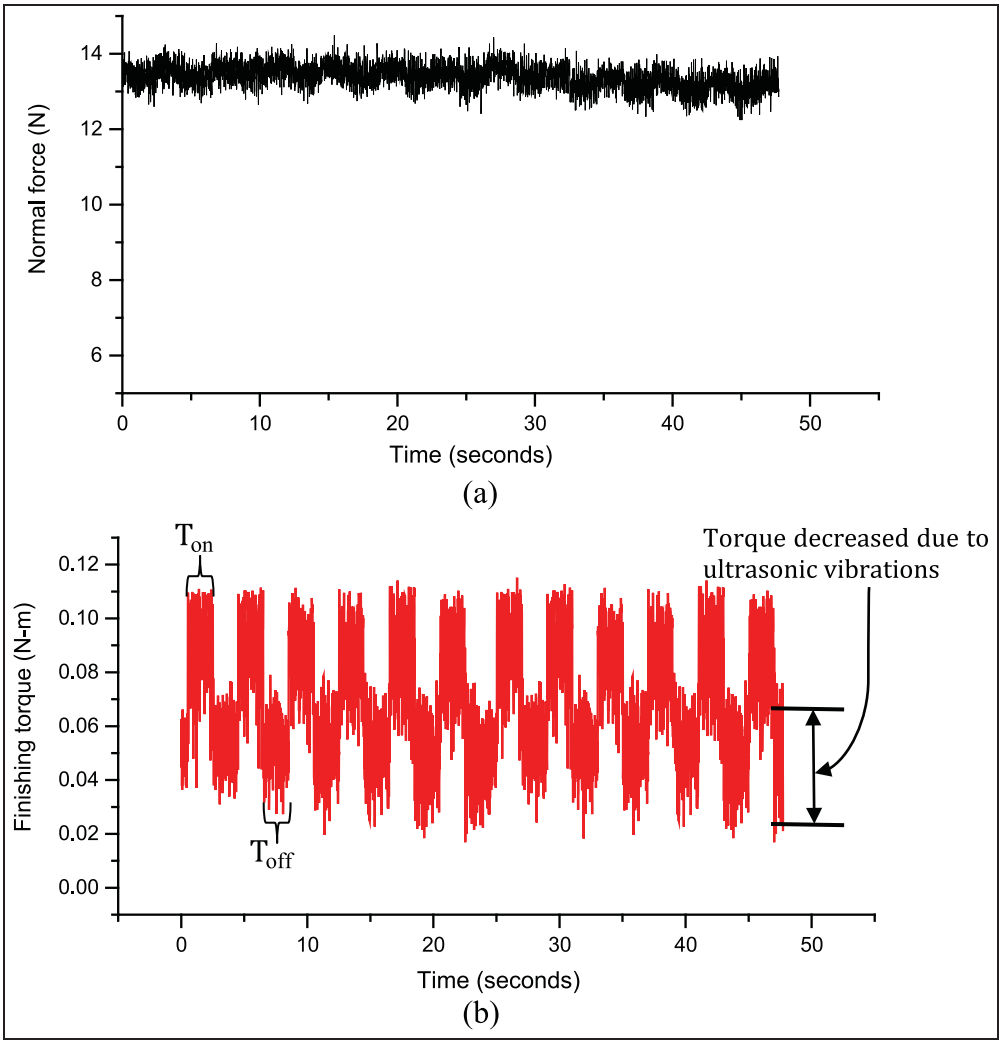

Figure 8. Variation of measured (a) normal force and (b) finishing torque with time, at 60 V, 1.5-mm gap T_{on} = 2 s and T_{off} = 2 s.

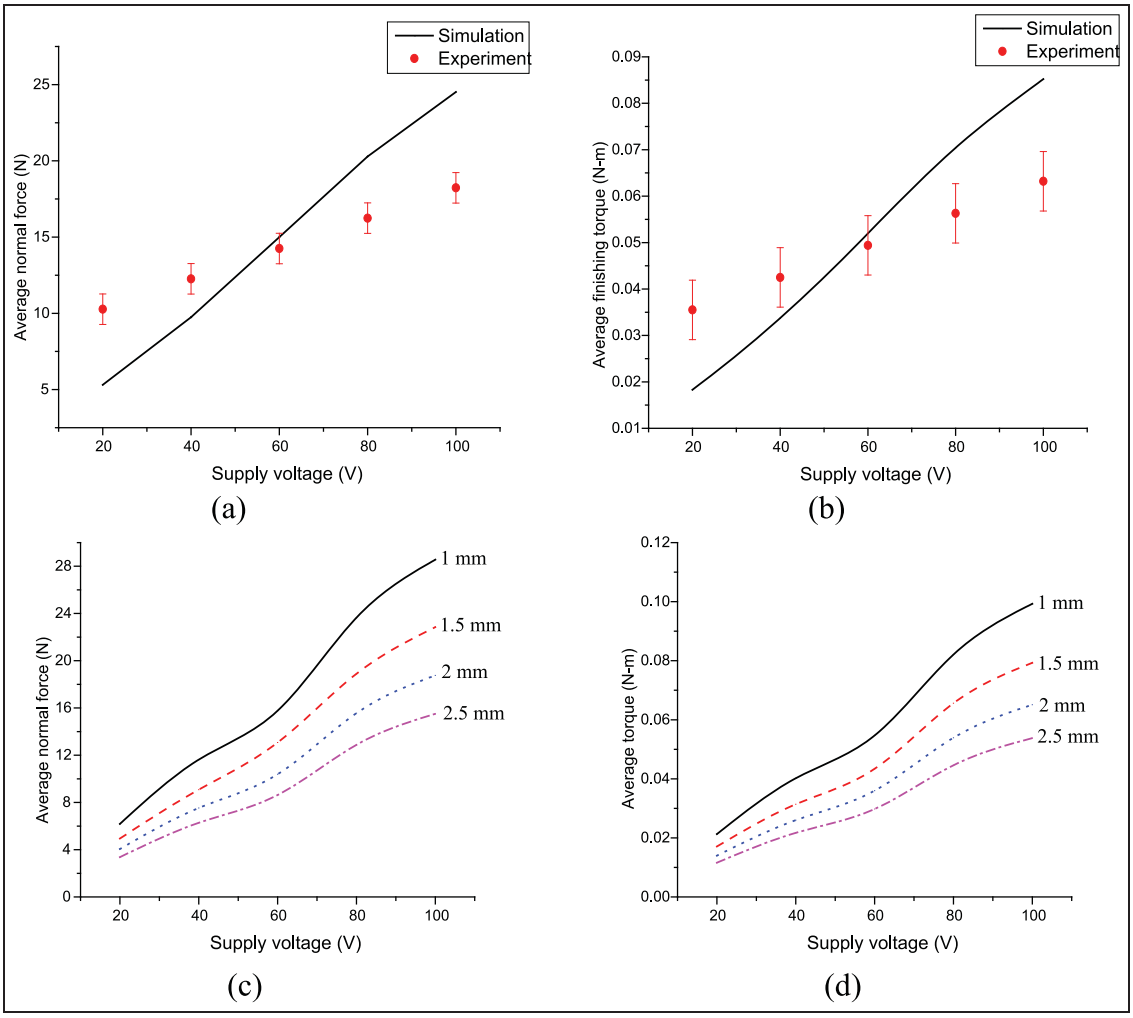

Figure 9. Comparison of experimental and predicted values of (a) average normal force and (b) average finishing torque during UAMAF gap of 1.5 mm; parametric analysis of (c) average normal force (d) average finishing torque for different values of supply voltage at varying working gap.

reaction force created by external support, but when the vibrations was stopped, workpiece still vibrated due to inertia and the torque produced was lower than that produced without vibration (Figure 8(b)). This reduction in torque is because of the reduction in friction force between the FMAB and the workpiece surface. The previous researchers[35,36] also suggested that there was a reduction in sliding friction on application of vibrations. The experimental values used to calculate the normal forces were the average over the whole period of time, but for average value of the finishing torque, only time T_{off} (i.e. without vibrations) was considered during the experimentation.

Results and discussion

To check the validity of the developed force model, the simulated values for the normal force and the finishing torque were compared with the experimental results. The material properties and machining parameters used in the simulations were as follows: density of SiC abrasive ($\rho_{abrasive}$) as 3210 kg/m^3, density of ferromagnetic particle as 7874 kg/m^3, relative permeability of ferromagnetic particles (μ_{FP}) as 1300, permeability of free space (μ_0) as 4×10^{-7} H/m[15] and relative permeability of abrasive grain (μ_{ABR}) as 0.999.[37] The size of abrasive and ferromagnetic particles were 400 and 300 mesh numbers, respectively. Amplitude and frequency vibration used were 8 μm and 20 kHz, respectively. The effects of various finishing parameters such as supply voltage, working gap, the concentration of abrasive in the FMAB on the normal force and the finishing torque for the UAMAF process are discussed below.

Voltage

In the UAMAF process, the input voltage to the electromagnet produced the magnetic field, controlling the magnetic pressure applied by the FMAB on the surface of the workpiece. Figure 9(a) and (b) demonstrates the comparison of calculated and experimental values of the average normal force and the finishing torque for

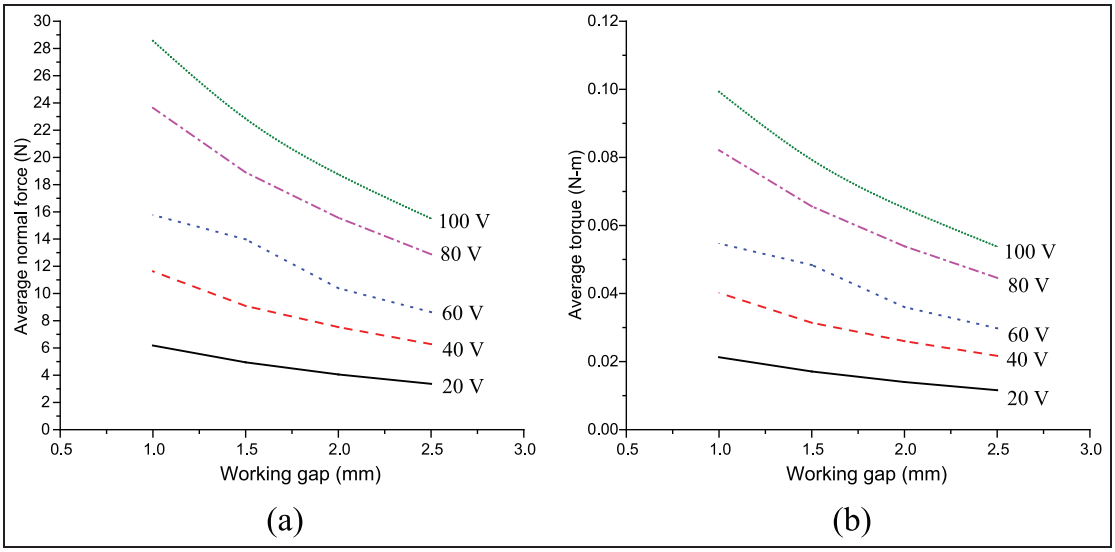

Figure 10. Effect of working gap on (a) averaged normal force and (b) averaged finishing torque during UAMAF for different supply voltages.

different levels of supply voltage. The effect of voltage on the average normal force is shown in Figure 9(a); it is observed that the force increased with voltage. This is attributed to the fact that with increased voltage, the average magnetic flux density in the finishing gap increases, thus forming strong chains of ferromagnetic particles, causing an increase in the yield strength of the FMAB. Hence, active abrasive grains in FMAB create a higher normal force on the surface of the workpiece. The increased average normal force on active abrasive grains caused greater indentation of abrasive grains into the workpiece surface; hence, the torque required to rotate the brush increased (Figure 9(b)).

There is some deviation of theoretical results from experimental observations. At a lower voltage, abrasive and ferromagnetic particles were not rigidly held together. Hence, during finishing some abrasive particles dropped down from the FMAB and formed a micro-layer under it. Effectively, the finishing occurred with a much higher number of active abrasive particles than assumed. The magnetic levitation force acting on them produced relatively higher force. As the voltage increased, the FMAB gained the strength; also, the bonding strength between abrasive and ferromagnetic particles increased. The amount of actual active abrasive particles on the workpiece surface reduced. At a very high voltage, only a fraction of the calculated active abrasive particles acted on the surface. Also, the effect of vibrations reduced the normal force that was not accounted in the model. Hence, the calculated forces and torque were greater than experimentally observed values. Figure 9(c) and (d) shows the trends for average normal force and finishing torque with supply voltage at different working gaps as obtained in the simulations. It is concluded from the figure that the increasing gap at the fixed voltage results in a decrease in the normal force and the finishing torque.

Working gap

The working gap refers to the distance between the electromagnet and the surface of the workpiece in UAMAF. Figure 10 shows an increase in the average normal force and the finishing torque with a decrease in the working gap in UAMAF. It is due to the fact that a smaller working gap results in a higher magnetic flux density; hence, a higher magnetic pressure acted on the workpiece surface resulted in a higher normal force exerted by FMAB on the workpiece surface. The size of indentation of abrasive depends upon the normal force acting on it, and the radius of indentation affects the coefficient of friction (equations (16)–(19)) and, thereby, the finishing torque. Hence, the finishing torque also decreases with an increase in the working gap as observed from Figure 10(b).

Concentration of abrasives

The mass fraction of abrasive in the FMAB is the ratio of the mass of abrasive particles to the total mass of UMAPs (ferromagnetic and abrasive particles). The abrasive particles are generally of non-magnetic nature. Hence, their magnetic permeability is very small compared to that of ferromagnetic particles. The addition of abrasives to ferromagnetic particles will tend to reduce the magnetic permeability of the FMAB. Therefore, its magnetic permeability depends upon the magnetic permeability of ferromagnetic and abrasive particles and also on their individual quantity in UMAPs. The effect of mass fraction of abrasive particles in the FMAB on the average normal force is shown in Figure 11. Both parameters decreased with an increase in the mass fraction of abrasives. This was due to the fact that an increasing amount of abrasive particles in the FMAB reduces its relative magnetic

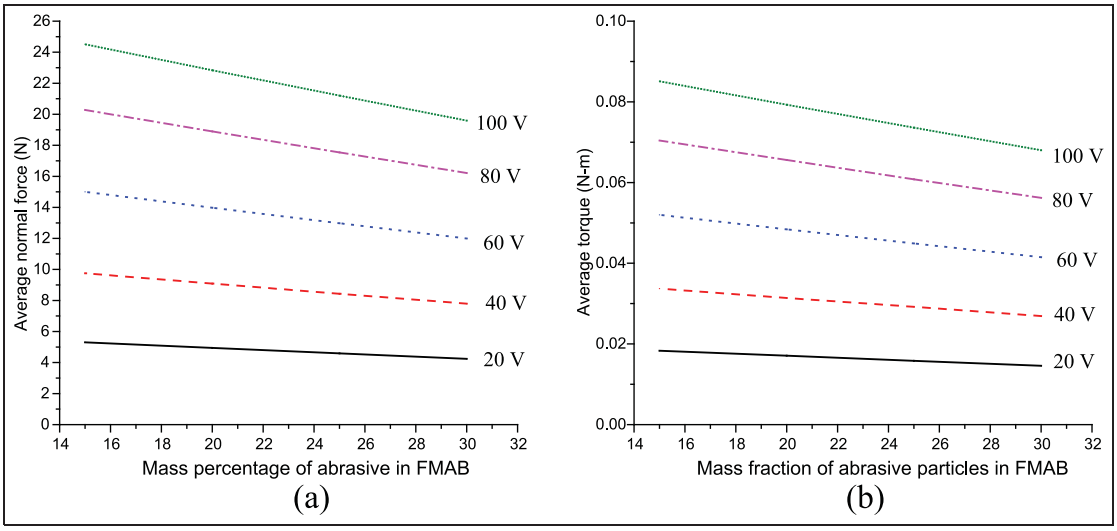

Figure 11. Effect of concentration of abrasives in FMAB on (a) average normal force and (b) average finishing torque during UAMAF for different supply voltages.

permeability. This reduction diminishes the rigidity of the FMAB and, hence, the force applied by it. Also, it can be concluded from Figure 11 that an increase in the voltage at the same mass fraction of abrasive particles causes an increase in the normal force and finishing torque.

Conclusion

In this work, a model of the electromagnet was created and finite element method (FEM) simulation was performed to assess the magnetic flux density on the surface of the workpiece. The theoretical models for the normal force and the finishing torque during UAMAF were also presented. The following outcomes are deduced from the presented analysis:

1. The simulation of the electromagnet predicted the magnetic flux density on the workpiece surface reasonably well.
2. It was established by means of mathematical modeling that the finishing torque was directly dependent on the normal force produced by the magnetic field.
3. The magnetic flux density on the workpiece surface decreased as the working gap increased and increased with supply voltage.
4. Increased supply voltage resulted in higher normal force and finishing torque.
5. Increased concentration of abrasive particles in FMAB reduced the normal force and the finishing torque of UAMAF.
6. The mathematical models for prediction of the normal force and the finishing torque were developed successfully based on the process physics. The developed models were validated with the obtained experimental results and found to be in reasonably good agreement.

Declaration of conflicting interests

The author(s) declared no potential conflicts of interest with respect to the research, authorship and/or publication of this article.

Funding

The author(s) disclosed receipt of the following financial support for the research, authorship, and/or publication of this article: This work was supported by the Department of Science and Technology (DST; India) and Engineering and Physical Sciences Research Council (EPSRC; United Kingdom) entitled "MAST: Modeling of Advanced Materials for Simulation of Transformative Manufacturing Processes" (grant identifications: DST/RC-UK/14-AM/2012 and EP/K028316/1).

References

1. Jain V. *Advanced machining processes*. New Delhi, India: Allied Publishers Pvt Limited, 2009.
2. Tan KL, Yeo S-H and Ong CH. Nontraditional finishing processes for internal surfaces and passages: a review. *Proc IMechE, Part B: J Engineering Manufacture*. Epub ahead of print 27 January 2016. DOI: 10.1177/0954405415626087.
3. Dong Z, Ya G and Liu J. Study on machining mechanism of high viscoelastic abrasive flow machining for surface finishing. *Proc IMechE, Part B: J Engineering Manufacture* 2017; 231: 608–617.
4. Gov K and Eyercioglu O. Effects of abrasive types on the surface integrity of abrasive-flow-machined surfaces. *Proc IMechE, Part B: J Engineering Manufacture*. Epub ahead of print 3 August 2016. DOI: 10.1177/0954405416662080.

5. Sarkar M and Jain VK. Nanofinishing of freeform surfaces using abrasive flow finishing process. *Proc IMechE, Part B: J Engineering Manufacture* 2017; 231: 1501–1515.
6. Sidpara A and Jain VK. Theoretical analysis of forces in magnetorheological fluid based finishing process. *Int J Mech Sci* 2012; 56: 50–59.
7. Dehghan Ghadikolaei A and Vahdati M. Experimental study on the effect of finishing parameters on surface roughness in magneto-rheological abrasive flow finishing process. *Proc IMechE, Part B: J Engineering Manufacture* 2015; 229: 1517–1524.
8. Ahn BW and Lee SH. Run-to-run process control of magnetic abrasive finishing using bonded abrasive particles. *Proc IMechE, Part B: J Engineering Manufacture* 2012; 226: 1963–1975.
9. Singh DK, Jain VK and Raghuram V. Parametric study of magnetic abrasive finishing process. *J Mater Process Tech* 2004; 149: 22–29.
10. Chang G-W, Yan B-H and Hsu R-T. Study on cylindrical magnetic abrasive finishing using unbonded magnetic abrasives. *Int J Mach Tool Manu* 2002; 42: 575–583.
11. Wang Y and Hu D. Study on the inner surface finishing of tubing by magnetic abrasive finishing. *Int J Mach Tool Manu* 2005; 45: 43–49.
12. Kim J-D and Choi M-S. Development of the magneto-electrolytic-abrasive polishing system (MEAPS) and finishing characteristics of a Cr-coated roller. *Int J Mach Tool Manu* 1997; 37: 997–1006.
13. Yan BH, Chang GW, Cheng TJ, et al. Electrolytic magnetic abrasive finishing. *Int J Mach Tool Manu* 2003; 43: 1355–1366.
14. Jain V. *Micromanufacturing processes*. Boca Raton, FL: CRC Press, 2013.
15. Mulik RS and Pandey PM. Experimental investigations and optimization of ultrasonic assisted magnetic abrasive finishing process. *Proc IMechE, Part B: J Engineering Manufacture* 2011; 225: 1347–1362.
16. Mulik RS and Pandey PM. Mechanism of surface finishing in ultrasonic-assisted magnetic abrasive finishing process. *Mater Manuf Process* 2010; 25: 1418–1427.
17. Shinmura T, Takazawa K, Hatano E, et al. Study on magnetic abrasive finishing. *CIRP Ann: Manuf Techn* 1990; 39: 325–328.
18. Khairy AB. Aspects of surface and edge finish by magnetoabrasive particles. *J Mater Process Tech* 2001; 116: 77–83.
19. Mori T, Hirota K and Kawashima Y. Clarification of magnetic abrasive finishing mechanism. *J Mater Process Tech* 2003; 143–144: 682–686.
20. Kim JD and Choi MS. Simulation for the prediction of surface-accuracy in magnetic abrasive machining. *J Mater Process Tech* 1995; 53: 630–642.
21. Jayswal SC, Jain VK and Dixit PM. Modeling and simulation of magnetic abrasive finishing process. *Int J Adv Manuf Tech* 2005; 26: 477–490.
22. Kala P, Sharma V and Pandey PM. Surface roughness modelling for Double Disk Magnetic Abrasive Finishing process. *J Manuf Process* 2017; 25: 37–48.
23. Mulik RS and Pandey PM. Experimental investigations and modeling of finishing force and torque in ultrasonic assisted magnetic abrasive finishing. *J Manuf Sci E: T ASME* 2012; 134: 051008.
24. Koshy P, Jain VK and Lal GK. Stochastic simulation approach to modelling diamond wheel topography. *Int J Mach Tool Manu* 1997; 37: 751–761.
25. Singh DK, Jain VK and Raghuram V. On the performance analysis of flexible magnetic abrasive brush. *Mach Sci Technol* 2005; 9: 601–619.
26. Jha S and Jain VK. Modeling and simulation of surface roughness in magnetorheological abrasive flow finishing (MRAFF) process. *Wear* 2006; 261: 856–866.
27. Das M, Jain VK and Ghoshdastidar PS. Analysis of magnetorheological abrasive flow finishing (MRAFF) process. *Int J Adv Manuf Tech* 2008; 38: 613–621.
28. Das M, Jain VK and Ghoshdastidar PS. Computational fluid dynamics simulation and experimental investigations into the magnetic-field-assisted nano-finishing process. *Proc IMechE, Part B: J Engineering Manufacture* 2012; 226: 1143–1158.
29. Bowden FP, Moore AJW and Tabor D. The plowing and adhesion of sliding metals. *J Appl Phys* 1943; 14: 80–91.
30. Goddard J and Wilman H. A theory of friction and wear during the abrasion of metals. *Wear* 1962; 5: 114–135.
31. Jain RK, Jain VK and Dixit PM. Modeling of material removal and surface roughness in abrasive flow machining process. *Int J Mach Tool Manu* 1999; 39: 1903–1923.
32. Jain VK, Kumar R, Dixit PM, et al. Investigations into abrasive flow finishing of complex workpieces using FEM. *Wear* 2009; 267: 71–80.
33. Pintaude G, Tanaka DK and Sinatora A. The effects of abrasive particle size on the sliding friction coefficient of steel using a spiral pin-on-disk apparatus. *Wear* 2003; 255: 55–59.
34. Budynas R and Nisbett J. *Shigley's mechanical engineering design*. 10th ed. New York: McGraw-Hill Education, 2015.
35. Kumar V and Hutchings I. Reduction of the sliding friction of metals by the application of longitudinal or transverse ultrasonic vibration. *Tribol Int* 2004; 37: 833–840.
36. Littmann W, Storck H and Wallaschek J. Sliding friction in the presence of ultrasonic oscillations: superposition of longitudinal oscillations. *Arch Appl Mech* 2001; 71: 549–554.
37. Judal KB and Yadava V. Modeling and simulation of cylindrical electro-chemical magnetic abrasive machining of AISI-420 magnetic steel. *J Mater Process Tech* 2013; 213: 2089–2100.

Appendix I

Notation

A	amplitude of ultrasonic vibration
A_{brush}	theoretical area of brush in contact with workpiece surface
A_w	Actual area of brush in contact with workpiece surface
A_p	area of the pole of electromagnet
B	average magnetic flux density
C	weight fraction of abrasives or concentration of abrasive by weight
D_a	diameter of abrasive particle
D_f	diameter of ferromagnetic particle
D_i	diameter of indentation

f	frequency of ultrasonic vibration
F_{au}	total average frictional force in UAMAF
f_0	friction force caused by single abrasive particle
f_N	average normal force acting on single abrasive particle
F_0	total friction force caused FMAB
F_N	averaged normal force exerted by FMAB
F_X	component of friction force along X-axis
F_Y	component of friction force along Y-axis
F_{xa}	resultant averaged friction force along X-axis during complete cycle of vibration
F_{ya}	resultant averaged friction force along Y-axis during complete cycle of vibration
H_w	Brinell hardness of workpiece material
K	constant
l	length of unit BCC cell
M, M_a, M_b	mesh number, lower mesh number, upper mesh number
n_a	number of active abrasive particles
N	r/min of electromagnet
P_m	averaged normal pressure
r_{inner}	innermost distance of pole from center of electromagnet
r_{mean}	mean radius of electromagnet
r_{outer}	outermost distance of pole from center of electromagnet
T	time period of vibration
T_{MAF}	torque produced without ultrasonic vibrations
T_{UAMAF}	torque acting during UAMAF
V_{brush}	volume of brush
V_{ferro}	volume of ferromagnetic particles in FMAB
V_r	tangential velocity of abrasive particle during rotation
V_{rr}	resultant velocity between velocity component V_y and V_u
$V_u(t)$	instantaneous velocity of ultrasonic vibration at time t
V_x	component of velocity of abrasive particle along X-axis
V_y	component of velocity of abrasive particle along Y-axis
α	volume fraction of ferromagnetic particles
η_b	factor taking into account deviation of actual area of brush that takes part in finishing as compared to area of pole of electromagnet
μ	coefficient of friction
μ_0	magnetic permeability in vacuum
μ_a	adhesion friction coefficient
μ_{ABR}	magnetic permeability of abrasive particles
μ_{brush}	magnetic permeability of FMAB
μ_{FP}	magnetic permeability of ferromagnetic particles
μ_p	plowing friction coefficient
$\rho_{abrasive}$	density of abrasive particle
ρ_{brush}	density of flexible magnetic abrasive brush
ρ_{ferro}	density of ferromagnetic particle
σ_w	flow stress of workpiece material